Clinical Radiology 74 (2019) 653.e1–653.e9

Contents lists available at ScienceDirect

Clinical Radiology

journal homepage: www.clinicalradiologyonline.net

Small hepatocellular carcinoma: using MRI to predict histological grade and Ki-67 expression

Y. Li [a,*,1], J. Chen [a,1], S. Weng [b], H. Sun [a], C. Yan [a], X. Xu [a], R. Ye [a], J. Hong [c]

[a] Department of Radiology, First Affiliated Hospital of Fujian Medical University, Fuzhou, Fujian, 350005, China
[b] Department of Radiology, Fujian Provincial Maternity and Child Health Hospital, Fuzhou, Fujian, 350001, China
[c] Key Laboratory of Radiation Biology (Fujian Medical University), Fujian Province University; Department of Radiation Oncology, The First Affiliated Hospital of Fujian Medical University, Fuzhou, Fujian 350005, China

ARTICLE INFORMATION

Article history:
Received 11 December 2018
Accepted 16 May 2019

AIMS: To investigate the predictive indicators of small aggressive hepatocellular carcinomas by examining the association between preoperative magnetic resonance imaging (MRI) parameters and Ki-67 expression and histological grade.

MATERIALS AND METHODS: Sixty patients with small hepatocellular carcinomas (tumour diameter: ≤3 cm, tumour numbers: ≤2) who underwent curative resection or biopsy after contrast-enhanced and diffusion-weighted MRI were evaluated retrospectively. Signal intensity (SI) of the whole lesion and erector spinae muscle was measured quantitatively. Tumour-to-muscle SI ratio was calculated. The association between these MRI parameters and histological grade and Ki-67 level was then investigated.

RESULTS: There was a significant correlation between tumour-to-muscle SI ratio and histological grade in tissues captured during the non-enhanced T1-weighted (p=0.001), arterial phase (p=0.001), and portal venous phase (p=0.036) of dynamic contrast-enhanced MRI and apparent diffusion coefficient (p=0.027). Arterial inhomogeneous enhancement was also correlated with high-Ki-67 expression (p=0.032).

CONCLUSIONS: Preoperative MRI may serve as a non-invasive tool for prediction of small, aggressive hepatocellular carcinomas, which may otherwise be treated conservatively.

© 2019 The Royal College of Radiologists. Published by Elsevier Ltd. All rights reserved.

Introduction

Hepatocellular carcinoma (HCC) is the fifth most common malignancy and the third most common cause of cancer-related deaths worldwide.[1–4] Due to the poor prognosis for patients with HCC, it is crucial to identify HCC at an early stage and select the optimal treatment in order to achieve satisfactory outcome. Cirrhosis is the most important clinical risk factor for HCC, and approximately 80% of cases of HCCs develop against a background of cirrhotic liver.[5] Studies have showed that human hepatocarcinogenesis involves the stepwise progression of the tumour from a high-grade dysplastic nodule (DN) in a cirrhotic liver to advanced HCC.[6–8] With the optimisation of medical imaging technologies, especially the widely use of magnetic resonance imaging (MRI), the rate of early detection is increasing, especially for small HCC (≤3 cm).

* Guarantor and correspondent: Y. Li, Department of Radiology, the First Affiliated Hospital of Fujian Medical University, Fuzhou, 350005, Fujian Province, China. Tel.: +8618959172818.
E-mail address: fjmulym@163.com (Y. Li).
[1] These authors contributed equally to this work and are co-first authors.

https://doi.org/10.1016/j.crad.2019.05.009
0009-9260/© 2019 The Royal College of Radiologists. Published by Elsevier Ltd. All rights reserved.

Although small HCCs usually have better outcomes than larger HCCs, a subset of small HCCs have been identified as more aggressive, with poorer clinical prognosis. Investigators have reported that the histological grade of HCCs is a valuable prognostic factor; higher histological grades indicate worse survival probability.[9,10] The nuclear protein, Ki-67, is associated with cell proliferative activity, which may be an indicator of tumour aggressiveness, and is expressed in all phases of the cell cycle except G0, with particularly high expression observed in the G2/M phase.[11] High expression of Ki-67 is associated with a higher tumour grade[12] and higher mortality.[13] Studies have showed that patients with a higher level of Ki-67 expression had a worse prognosis.[14,15] Identification of small HCCs with high histological grade or high Ki-67 expression may help in the selection of appropriate treatment, improving remission rates. The caveat of these prognostic factors is that neither the histological grade nor Ki-67 expression is routinely available through biopsy due to the invasiveness and concern of procedure-related complications. As such, there is a need for non-invasive methods to evaluate Ki-67 expression or histological grade.

Studies have evaluated the correlation between blood supply and histological grade for HCCs,[6,16,17] some demonstrated that the arterial blood supply decreases as the histological grade progresses in the late stage of HCC development (17). Signal intensity (SI) in dynamic contrast-enhanced MRI was hypothesised to help predict histological grade. Huang *et al.* reported that apparent diffusion coefficient (ADC) values are significantly negatively correlated with Ki-67 expression,[18] but for small HCCs, the correlation between them remains unknown. The purpose of the present study was to investigate the association between histological tumour grade and Ki-67 expression and a battery of preoperative MRI findings, including quantitative and qualitative parameters, for the detection of aggressive small HCCs.

Material and methods

Patient population

The study protocol conformed to the ethical guidelines of the Declaration of Helsinki as reflected in a priori approval by the institutional review board, who waived the requirement for informed consent. Patient medical records were reviewed between January 2011 and December 2017 and 949 patients with histopathologically confirmed HCCs (by surgery or biopsy) were identified. The patients were included consecutively according to the following inclusion criteria[1]: undergoing routine immunochemical staining for Ki-67 (n=484)[2]; diffusion-weighted imaging (DWI) and dynamic-enhanced MRI performed before surgery or biopsy and tumour diameter: ≤3 cm, tumour number: ≤2 (n=71). Of the 71 retrieved patients, 11 were subsequently excluded for the following reasons[1]: prior local–regional therapy such as chemoembolisation, radiofrequency ablation, or chemotherapy and radiation therapy before surgery or biopsy (n=5)[2]; an interval >1 month between MRI examination and surgery or biopsy (n=4)[3]; suboptimal image quality for interpretation (n=2). Finally, a total of 60 patients were included (Fig 1), consisting of 51 males and nine females (mean age, 55 years; range, 20–82 years). In patients with multifocal lesions, the largest lesion was chosen as the study target (60 lesions in total). Alpha-fetoprotein (AFP) examination was also performed before MRI examination.

Histopathological analysis

Of the 60 selected HCC lesions, three were confirmed at biopsy and 57 were confirmed at surgery. The histopathological examination was performed by an experienced pathologist who was blinded to radiological and clinical results. The major histological grade of HCC (predominant grade within the tumour) was recorded as well-differentiated (WD), moderately differentiated (MD), or poorly differentiated (PD) HCC.

Ki-67 was assessed using paraffin-embedded tissue samples, which were cut into 4-μm-thick sections. Briefly, all sections were deparaffinised and antigen was retrieved under high pressure for 120 seconds. Non-specific binding was blocked by serum at 37°C for 15 minutes (Beijing Zhongshan Golden Bridge Biotechnology Company, China). The tumour tissue sections were stained with primary monoclonal mouse anti-human Ki-67 antibody (Beijing Zhongshan Golden Bridge Biotechnology Company, China; Clone no. MIB-1) in a humidified chamber at 37°C for 30 minutes. Then the specimens were incubated with secondary goat anti-mouse antibody at 37°C for 30 min. Ki-67 expression were visualised using 3,3′-diaminobenzidine (DAB) followed by counterstaining with haematoxylin. The Ki-67 labelling index was evaluated by calculating the frequency of Ki-67 positive cells. Ki-67 was considered positive when the cell nuclei were stained brown–yellow. Immunoreactive cells were classified as low (10% or less immunoreactivity) or high (>10% immunoreactivity).[13]

MRI protocol

MRI images were acquired using a 3-T MRI system (Magnetom Verio; Siemens Healthcare, Erlangen, Germany) with an eight-channel body phased-array coil. The mean time interval between MRI examination and surgical resection or biopsy was 9.85±7.14 days (range 1–30 days). The sequences of non-enhanced MR images included: a respiration-triggered T2-weighted fat-suppression turbo spin-echo sequence (6,500–7,000 ms repetition time [TR], 79 ms echo time [TE], 240 Hz/pixel bandwidth, 320×224 matrix size, 5 mm section thickness, 1 mm intersection gap), a breath-hold T1-weighted gradient-echo in-phase sequence (133 ms TR, 6.2 ms TE, 280 Hz/pixel bandwidth, 320×224 matrix size), an out-of-phase sequence (133 ms TR, 2.5 ms TE, 280 Hz/pixel bandwidth, 320×224 matrix size), DWI with the respiratory triggered sensitivity encoding technique (6,300 ms TR, 93 ms TE; gradient factor b-values of 50 and 800 s/mm^2, 170 mm matrix size, 3 mm

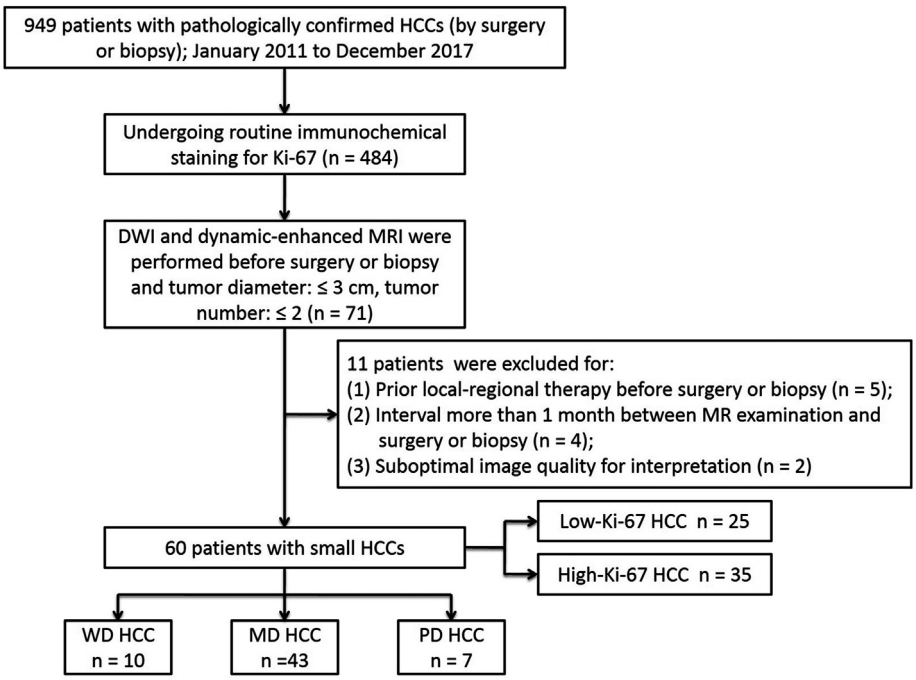

Figure 1 Flow diagram shows inclusion and exclusion criteria for the study. WD = well differentiated, MD = moderately differentiated, PD = poorly differentiated.

slice thickness), ADC maps (obtained by using a mono-exponential function with b-values of 50 and 800 s/mm^2), and T1-weighted three-dimensional volumetric interpolated breath-hold examination gradient-echo sequence with fat suppression (3.9 ms TR, 1.4 ms TE, 400 Hz/pixel bandwidth, 320×224 matrix size, 3 mm slice thickness, no gap). For dynamic contrast-enhanced MRI, Gd-BOPTA was administered intravenously using a power injector at 2 ml/s for total dose of 0.1 mmol/kg and followed by 20 ml saline flush. Dynamic contrast-enhanced images, including the arterial phase (20–25 seconds), portal venous phase (60–70 seconds) and transitional phase (2 minutes), were acquired using a T1-weighted three-dimensional volumetric interpolated breath-hold examination with the same parameters.

Qualitative and quantitative analyses

All HCC MRIs were reviewed independently by two senior abdominal radiologists with 30 and 20 years of experience, respectively. Interpretation was guided by using the picture archiving and communication system (PACS). Both observers were blinded to clinical, laboratory, and histopathological results. MRI features were first evaluated independently. Subsequently, the two reviewers met to finalise decisions for discrepant results.

The following imaging parameters were qualitatively evaluated: (1) irregular tumour margin, defined as non-smooth margin with a budding portion at the tumour periphery on transverse images; (2) typical enhancement pattern, defined as arterial enhancement with washout on portal venous or transitional phase; (3) arterial rim enhancement, defined as presence of irregular ring-like areas of enhancement with central hypointense areas in arterial phase; (4) arterial inhomogeneous enhancement; (5) intratumoural fat, defined as tumour area with decreased signal intensity on opposed-phase images compared with in-phase images; and (6) tumour capsule, defined as a distinct low SI rim on arterial phase images with delayed contrast enhancement surrounding tumour margin.

Quantitative analysis was performed by a radiologist. Lesion size was measured by recording the maximum dimension for each tumour on T2-weighted axial image where the tumour had the largest cross-sectional diameter (3/60 HCCs were measured on other sequences as they were undetected on T2-weighted axial image). The SI of the tumours (TSI) was measured using a region of interest (ROI) on pre-contrast MRI, post-contrast MRI, and ADC maps at the same level of the largest diameter of the tumour in the axial plane with a maximum area. Regions of interest were manually positioned to include almost the entire HCC area. Because a few lesions were not visualised well in some sequences, other sequences were reviewed for the accurate placement of the ROI on the lesion by visual correlation of the image sets. The SI of the right erector spinae muscle was also measured as a reference in the ROI (approximately 50–100 mm^2) in the same section.[19] HCCs often develop on a background of liver cirrhosis, which leads to inhomogeneous MRI images. To prevent this, the SI of unaffected liver parenchyma was not chosen as a reference. The SI of the lesions and erector spinae muscle were measured three times and averaged. In addition, another ROI (approximately 28 mm^2) was drawn on the ADC maps at the darkest area of HCCs and the result was marked as ADCmin value (Fig 2).

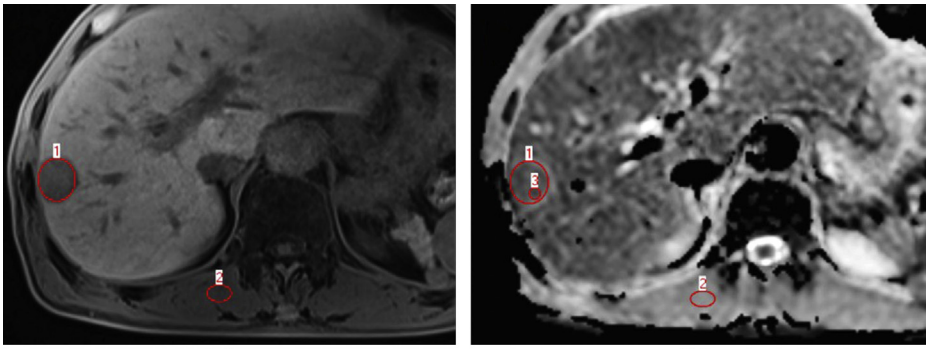

Figure 2 An example of MR images in the non-enhanced T1WI (a) and ADC map (b) to display the placement of ROIs for the measurement of signal intensities. A small ROI was drawn additionally on the ADC map (b) at the darkest area of the HCC.

Based these quantitative measurements, the tumour-to-muscle SI ratio (TMSI) in each sequence was defined as follows:

$$TMSI = TSI/MSI$$

TMSI on ADC maps was marked as ADC-TMSI and ADCmin-TMSI. In addition, TMSI on non-enhanced T1-weighted image (T1WI), arterial phase, portal venous phase and transitional phase was marked as N-TMSI, AP-TMSI, PVP-TMSI, and TP-TMSI, respectively. The relative enhancement (RE) was calculated as follows:[20]

$$RE = (\text{Post-enhancement TMSI} - \text{Pre-enhancement TMSI})/\text{Pre-enhancement TMSI}$$

Furthermore, RE on arterial phase, portal venous phase and transitional phase was marked as AP-RE, PVP-RE, and TP-RE, respectively.

Statistical analysis

Chi-square test or Fisher's exact test was used to analyse the correlation between categorical variables and Ki-67 expression or histological grade of small HCCs. Student's *t*-test or one-way analysis of variance (one-way ANOVA) was performed for continuous variables, then Bonferroni's test was used to identify the difference between each two groups. Spearman's correlation analysis was also used to assess the correlation between histological grade and quantitative variables. Additionally, the present study also divided the 60 small HCCs into two groups, one was poorly differentiated HCCs group, and the other group included the remaining HCCs. By using receiver operating characteristic (ROC) analysis, the appropriate cut-offs for quantitative variables corresponding to maximal Youden index were determined to identify the poorly differentiated small HCCs. Results were reported as mean ± standard deviation (SD) for continuous variables; numbers and percentages are shown for categorical variables. All statistical analyses were performed by SPSS Statistics version 22 and MedCalc Statistical Software version 15.6.1, Fuzhou, Fujian, China. The significance level was indicated by $p<0.05$ (two-tailed).

Results

Demographic and pathologic characteristics of small HCCs

Baseline demographic and pathological characteristics (Table 1) demonstrated that 10 of the 60 HCCs examined were well-differentiated (WD) HCCs, 43 were moderately differentiated (MD) HCCs, and seven were poorly differentiated (PD) HCCs. Twenty-five of the 60 HCCs had low Ki-67 expression, and the remaining 35 HCCs had high Ki-67 expression. Tumour size (1.93±0.61 cm) ranged from 0.67 to 3 cm in diameter. There were 34 lesions had an AFP value of <20 ng/ml, and the remaining 26 lesions had a value of ≥20 ng/ml. The relationship between AFP level and histological grade was significant, where AFP level was significantly lower in WD HCCs compared to MD and PD HCCs ($p=0.006$); however, AFP level was not significantly associated with Ki-67 expression ($p=0.66$). Spearman's correlation analysis further demonstrated that Ki-67 expression was positively correlated with histological grade ($p=0.049$, $\rho = 0.255$).

MRI characteristics related to histological grade

Upon qualitative analysis (Table 2), arterial rim enhancement and histological grade demonstrated a significant correlation ($p=0.049$), where higher histological grades more frequently showed arterial rim enhancement. Irregular tumour margin was also more frequently observed in the higher histological grade ($p=0.036$). Typical enhancement pattern, arterial inhomogeneous enhancement, tumour capsule, and intratumoural fat were not significantly associated among WD, MD, and PD HCCs.

The relationships between RE, TMSI, ADC value, ADCmin value, and each histological grade are shown in Table 3. The N-TMSI ($p=0.001$), AP-TMSI ($p=0.001$), PVP-TMSI ($p=0.036$), ADCmin-TMSI ($p=0.027$), and ADCmin value ($p=0.034$) were all significantly correlated with histological grade. As shown in Fig 3, the N-TMSI and AP-TMSI for PD HCCs were both significantly lower than that for WD ($p<0.001$, $p=0.001$, respectively) and MD ($p=0.029$, 0.048,

Table 1
Demographic and pathologic characteristics of small HCCs.

Variable	WD	MD	PD	*p*-Value	Low-Ki-67	High-Ki-67	*p*-Value
	n=10	*n*=43	*n*=7		*n*=25	*n*=35	
Age (years)	60.3±8.6	55.2±13.1	45.7±18.1	0.087	55.6±15.5	54.5±12.2	0.78
Gender				0.301			0.582
Male	7	38	6		20	31	
Female	3	5	1		5	4	
HBV infection				0.164			0.898
Absent	3	5	0		4	4	
Present	7	38	7		21	31	
AFP				0.006			0.66
<20 ng/ml	10	21	3		15	19	
≥20 ng/ml	0	22	4		10	16	
Cirrhosis				0.305			0.199
Absent	3	5	1		6	3	
Present	7	38	6		19	32	
Tumour location				0.991			0.529
Left	3	12	2		6	11	
Right	7	31	5		19	24	
Size (cm)	2.04±0.70	1.90±0.56	1.93±0.80	0.821	2.04±0.65	1.84±0.57	0.216

Data are expressed as mean ± standard deviation (SD) or numbers of patients.
WD, well differentiated; MD, moderate differentiated; PD, poorly differentiated; HBV, hepatitis B virus; AFP, alpha-fetoprotein.

Table 2
Qualitative MRI findings related to histological grade and Ki-67 expression.

Variable	WD	MD	PD	*p*-Value	Low Ki-67	High Ki-67	*p*-Value
	n=10	*n*=43	*n*=7		*n*=25	*n*=35	
Typical enhancement pattern				0.642			0.43
Absent	2	11	3		8	8	
Present	8	32	4		17	27	
Arterial inhomogeneous enhancement				0.469			0.032
Absent	6	23	2		17	14	
Present	4	20	5		8	21	
Tumour capsule				0.897			0.45
Absent	7	32	6		20	25	
Present	3	11	1		5	10	
Intratumoural fat				0.999			0.999
Absent	9	40	7		23	33	
Present	1	3	0		2	2	
Arterial rim enhancement				0.049			0.19
Absent	9	36	3		22	26	
Present	1	7	4		3	9	
Irregular tumour margin				0.036			0.226
Absent	8	33	2		20	23	
Present	2	10	5		5	12	

Data represent numbers of patients.
WD, well differentiated; MD, moderate differentiated; PD, poorly differentiated.

respectively) HCCs, which were also significantly different from each other (p=0.03, 0.016, respectively; Fig 4). The ADCmin value, ADCmin-TMSI, and PVP-TMSI for PD HCCs were lower than that for WD HCCs significantly (p=0.031, 0.025, 0.036, respectively); however, there were no differences between MD and WD or PD HCCs (p>0.05 for all). Additionally, the correlation analysis showed that the ADCmin value (p=0.019, ρ=−0.301), ADCmin-TMSI (p=0.017, ρ=−0.307) N-TMSI (p<0.001, ρ=−0.45), AP-TMSI (p<0.001, ρ=−0.459), and PVP-TMSI (p=0.007, ρ=−0.342) were all negatively correlated with tumour histological grade. However, ADC-TMSI, ADC value, AP-RE, PVP-RE and TP-RE were not significantly different in WD, MD and PD HCCs (p=0.135, 0.147, 0.590, 0.747, 0.388, respectively).

ROC curves of the ADCmin value, ADCmin-TMSI, N-TMSI, AP-TMSI and PVP-TMSI for the prediction of PD HCCs, and the AUCs were 0.728, 0.729, 0.814, 0.822 and 0.815, respectively (Fig 5). For predicting PD HCCs, the best cut-off points for these values were 0.58×10^{-3} mm^2/s, 0.34, 1.05, 1.50, and 1.28, respectively. The AP-TMSI was the optimal predictor of the presence of PD HCCs. The sensitivity and specificity of AP-TMSI for the prediction of PD HCCs were 85.7% and 75.5% respectively.

MRI characteristics related to Ki-67 expression

Qualitative analyses of MRI parameters are presented in Table 2. Arterial inhomogeneous enhancement was more

Table 3
Quantitative magnetic resonance imaging findings related to histological grade and Ki-67 expression.

Variable	WD	MD	PD	*p*-Value	Low Ki-67	High Ki-67	*p*-Value
	n=10	*n*=43	*n*=7		*n*=25	*n*=35	
N-TMSI	1.22±0.24	1.01±0.22	0.77±0.18	0.001	1.05±0.30	1.00±0.20	0.42
AP-TMSI	2.01±0.41	1.67±0.52	1.18±0.35	0.001	0.71±0.45	0.63±0.44	0.48
PVP-TMSI	1.78±0.44	1.62±0.48	1.20±0.30	0.036	0.67±0.41	0.53±0.36	0.19
TP-TMSI	1.67±0.30	1.49±0.40	1.25±0.32	0.910	0.58±0.39	0.43±0.31	0.10
AP-RE	0.75±0.35	0.67±0.47	0.53±0.32	0.590	1.76±0.58	1.63±0.50	0.35
PVP-RE	0.51±0.43	0.61±0.40	0.57±0.25	0.747	1.69±0.50	1.53±0.45	0.21
TP-RE	0.41±0.32	0.49±0.34	0.64±0.37	0.388	1.58±0.35	1.43±0.41	0.15
ADC-TMSI	0.80±0.13	0.72±0.24	0.58±0.23	0.135	0.74±0.25	0.70±0.21	0.48
ADC_{min}-TMSI	0.68±0.15	0.59±0.19	0.41±0.27	0.027	0.61±0.20	0.57±0.20	0.46
ADC ($\times 10^{-3}mm^2/s$)	1.125±0.143	1.023±0.293	0.853±0.317	0.147	1.018±0.227	1.022±0.319	0.96
ADC_{min} ($\times 10^{-3}mm^2/s$)	0.948±0.180	0.841±0.251	0.611±0.380	0.034	0.839±0.226	0.827±0.300	0.86

TMSI on non-enhanced T1 weighted image, arterial phase (AP), portal venous phase (PVP) and transitional phase (TP) was marked as N-TMSI, AP-TMSI, PVP-TMSI, and TP-TMSI, respectively.
RE = (Post-enhancement TMSI − Pre-enhancement TMSI)/Pre-enhancement TMSI.
Datas are expressed as mean±standard deviation (SD).
WD, well differentiated; MD, moderate differentiated; PD, poorly differentiated; TSI, signal intense of lesion; MSI, signal intense of muscle; TMSI = TSI/MSI.

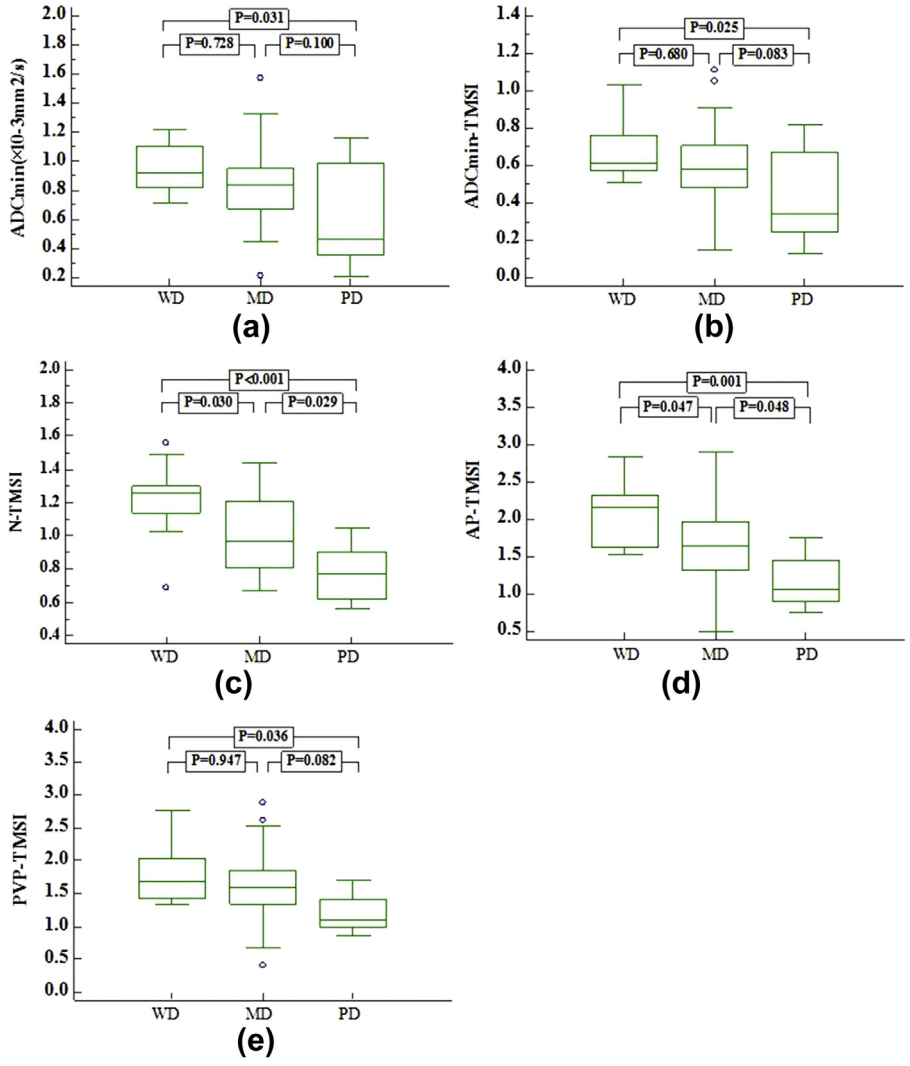

Figure 3 Correlations between histological grade (WD, well differentiated; MD, moderate differentiated; PD, poorly differentiated) and ADCmin value (a), ADCmin-TMSI (b), N-TMSI (c), AP-TMSI (d) and PVP-TMSI (e) in HCCs (TMSI, tumour-to-muscle signal intensity ratio, N, non-enhanced T1-weighted image, AP, arterial phase, PVP, portal venous phase, ADCmin, ADC values in small ROIs). The TMSI tends to drop off as the progression of differentiation degree in each phase, particularly in N and AP image.

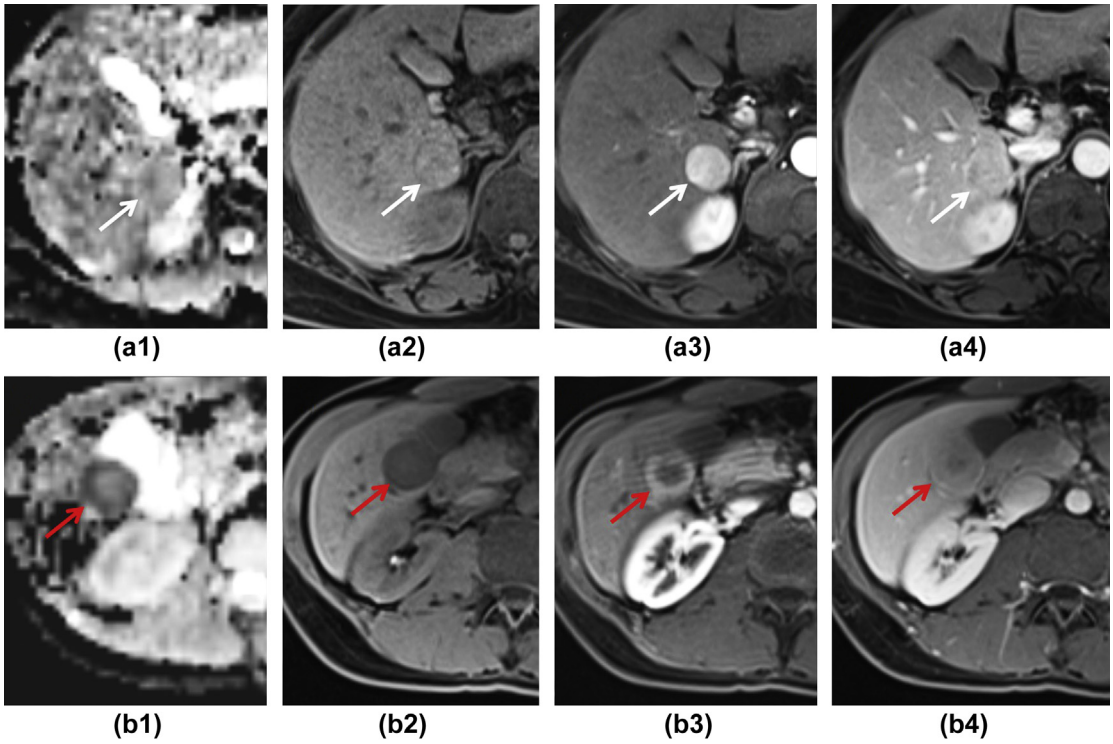

Figure 4 A well differentiated HCC (a1-4) and a poorly differentiated HCC (b1-4). On non-enhanced T1WI (a2, b2), arterial phase (a3, b3) and portal venous phase (a4, b4) of dynamic contrast-enhanced MRI images and ADC map (in a small ROI) (a1, b1), the signal intense of the lesion in a 59-year-old woman (a1–4) was higher than that in a 60-year-old man (b1–4). By measurement, TMSI (lesion to erector spinae muscle signal intense ratio) on these sequences was higher in the female as well.

predominant in HCCs with high Ki-67 expression than in those with low Ki-67 expression (p=0.032); however, typical enhancement pattern, tumour capsule, intratumoural fat, arterial rim enhancement, and irregular tumour margin were not significantly associated with Ki-67 expression. Neither ADC value, ADCmin value, TMSI, nor RE in each sequence was related to Ki-67 expression (Table 3).

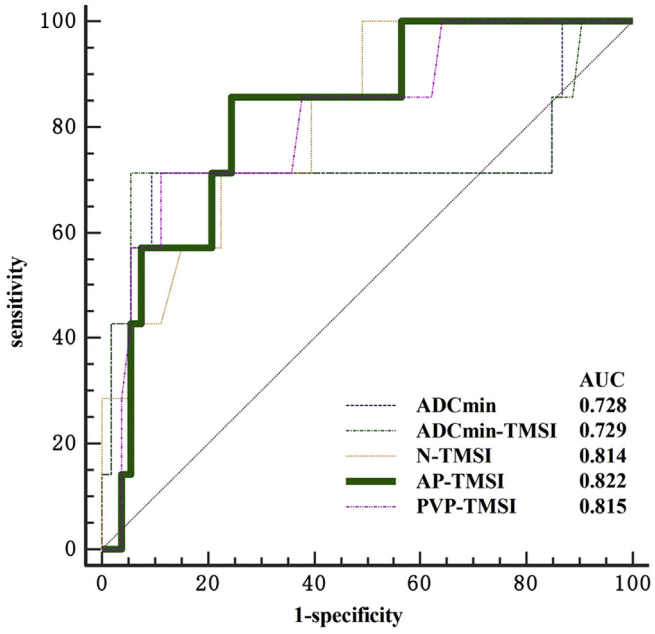

Figure 5 ROC curve of the ADCmin value, ADCmin-TMSI, N-TMSI, AP-TMSI and PVP-TMSI for the prediction of PD HCCs. The AUC values were 0.728, 0.729, 0.814, 0.822, and 0.815, respectively.

Discussion

This study demonstrated that AFP levels of the selected patients with small HCCs were associated with histological grade, where higher AFP levels were more frequently observed in tumours with higher histological grade, as supported by a previous study.[19] Arterial rim enhancement was observed more frequently in the higher histological grade HCCs, especially in MD and PD HCCs. Prior studies have described that arterial rim enhancement can be an indicator for poor differentiation and worse prognosis in HCCs.[21–23] Several studies have reported that histopathological absence of tumour capsule, infiltrative growth, and presence of microvascular invasion as well as rapid growth with central necrosis may all play a role in the observance of rim enhancement in HCC MRI.[21,24] The HCCs with higher histological grades more often manifested irregular tumour margins than HCCs with lower histological grades. This morphological characteristic is often demonstrated in various malignant tumours. Choi *et al.* demonstrated that pathological characteristics such as infiltrative, multifocal nodular confluence, or massive growth type might result in the appearance of these irregular tumour margins.[22] The present results were consistent with the previous study.

This study also suggested that N-TMSI, AP-TMSI, and PVP-TMSI values were all negatively correlated with histological grade, that is, lower SIs (refer to erector spinae muscle) were more often demonstrated in higher histological grade HCCs in non-enhanced T1WI, arterial and portal venous phase of dynamic contrast-enhanced MRI. Among the parameters, AP-TMSI was the optimal predictor for poorly differentiated HCCs. Correlation studies[6–8] have showed that during hepatocarcinogenesis, the density of portal triads diminishes while the density of unpaired arteries increases. The formation of unpaired neo-arteries increases arterial flow, which proposes that SI in arterial phase of dynamic contrast-enhanced MRI increases as histological grade grows; however, a previous study has suggested that arterial blood supply increases during the early stage of advancement but that, conversely, it decreases in the late stage of advancement.[17] Other studies have reported that the arterial blood supply of poorly differentiated HCCs is lower than that of moderately HCCs.[25,26] The present result was consistent with these latter studies. One explanation is that in advanced HCCs, rapid cell proliferation in the centre of the tumour elevates interstitial pressure, causing compression closure of tumour capillaries, and regression of neo-arteries.[6] The unpaired arteries, which provide nutrition for the tumour, are relatively immature in small HCCs, causing poor differentiation and leading to more weakly enhanced HCCs in arterial phase compared to well or moderately differentiated HCCs. The present study showed a decrease of PVP-TMSI in high histological grade tumours, which may be due to the diminishing density of portal triads. In the present study, the exact cause for the decrease of N-TMSI in high histological grade tumours is unknown. It is correlated with containing paramagnetic materials, such as copper or iron, which may increase the SI in T1-weighted images. Iron may accumulate within hepatocytes during the dysplastic phases of hepatocarcinogenesis. With progression to early and advanced HCC, iron usually regresses, causing the decrease of N-TMSI.

DWI is a MRI technique based on the measure of water diffusion in tissues.[27] ADC measurements obtained within DWI at two or more b-values further allow quantitative analysis of the diffusion.[28] The present study suggested that ADCmin value and ADCmin-TMSI were significantly negatively correlated with histological grade. Tumour cellular density and the nuclear/cytoplasmic ratio increase as the histological grade progresses, and may cause more markedly restrict diffusion, causing decreased ADC values (lower ADCmin and ADCmin-TMSI value in this study).[29,30] Some ADC parameters were found in this study to be some of the best predictors of PD HCCs. Specifically, the optimal cut-off points for sensitivity and specificity of ADCmin and ADCmin-TMSI were 0.58×10^{-3} mm^2/s and 0.34, respectively.

The nuclear Ki-67 protein is associated with cell proliferative activity. In this study, arterial inhomogeneous enhancement was more dominant in patients with high Ki-67 expression than in those with low Ki-67 expression. High expression of Ki-67 has been similarly associated with a higher tumour grade[12] and higher mortality[13] in previous studies. The correlation may be caused by the fact that HCCs with high expression of Ki-67 grow heterogeneously, where cell and vessel density is inhomogeneous. Despite this, among the quantitative MRI findings (ADC value, ADCmin value, TMSI, and RE) in each sequence, none were significantly associated with Ki-67 expression. Huang *et al.* reported that the ADC value was correlated with Ki-67 expression in HCC.[18] Some studies similarly showed that ADC values in different tumours were inversely correlated with Ki-67 expression.[31,32] The results of the present were not consistent with these studies. The discrepancy is possibly due to different populations of subjects across the studies. The present study sample consisted of relatively small HCCs, which differed from the HCCs of focus in the aforementioned studies. Despite sample differences, a meta-analysis has concluded that the correlation between ADC and Ki-67 is weak in hepatocellular carcinoma, making ADC an unlikely surrogate biomarker of cell proliferation in HCCs.[33] Other studies investigating the association of Ki-67 in various tumours have been inconsistent, with some authors describing that ADC fractions can be associated with cellular proliferation and others concluding the absence of such confirmation.[34–36] The exact causes of these discrepancies remain to be investigated.

The present study has several limitations. First, this study had a relatively small number of poorly differentiated HCCs (11.7% [7 of 60]), which may have diluted the true representation of the class. It may have been insufficient for assessing statistical significance among histological grade and, as such, predictive factors should be confirmed by a larger study. Second, measurement errors on each sequence were inevitable, especially for small lesions. Measurements were taken three times and averaged to minimise errors. Third, a survival analysis is needed in order to corroborate the clinical significance of the novel predictive factors outlined herein.

In summary, arterial rim enhancement, irregular tumour margin, low TMSI on non-enhanced T1WI, arterial phase, and portal venous phase of dynamic contrast-enhanced MRI and ADC maps (in a small ROIs) may be helpful predictors of poorly differentiated small HCCs, an aggressive subclass related to poor prognosis. Additionally, arterial inhomogeneous enhancement may predict small, aggressive HCCs with high Ki-67 expression. Thus, it is proposed that MRI examination is a non-invasive tool to obtain preoperative information about the tumour characteristics that can aid in the selection of appropriate anti-cancer treatments, improving remission rates.

Conflict of interest

The authors declare no conflict of interest.

Acknowledgements

This study received funding from the Fujian Provincial Health and Family Planning Commission (CN; award number: 2017-CX-27), Fujian Provincial Department of Science

and Technology (CN; award number: 2015J0105), and Fujian Medical Elite Cultivation Program (CN; award number: 2015-ZQN-ZD-19).

References

1. Wang T, Liu M, Zheng SJ, *et al*. Tumour-associated autoantibodies are useful biomarkers in immunodiagnosis of alpha-fetoprotein-negative hepatocellular carcinoma. *World J Gastroenterol* 2017;**23**(19):3496–504.
2. McGlynn KA, Petrick JL, London WT. Global epidemiology of hepatocellular carcinoma: an emphasis on demographic and regional variability. *Clin Liver Dis* 2015;**19**(2):223–38.
3. Hao Y, Numata K, Ishii T, *et al*. Rate of local tumour progression following radiofrequency ablation of pathologically early hepatocellular carcinoma. *World J Gastroenterol* 2017;**23**(17):3111–21.
4. Yang JD, Roberts LR. Epidemiology and management of hepatocellular carcinoma. *Infect Dis Clin N Am* 2010;**24**(4):899–919 [viii.].
5. McGlynn KA, London WT. Epidemiology and natural history of hepatocellular carcinoma. *Best Pract Res Clin Gastroenterol* 2005;**19**(1):3–23.
6. Choi JY, Lee JM, Sirlin CB. CT and MRI diagnosis and staging of hepatocellular carcinoma: part I. Development, growth, and spread: key pathologic and imaging aspects. *Radiology* 2014;**272**(3):635–54.
7. Matsui O. Imaging of multistep human hepatocarcinogenesis by CT during intra-arterial contrast injection. *Intervirology* 2004;**47**(3–5):271–6.
8. Narsinh KH, Cui J, Papadatos D, *et al*. Hepatocarcinogenesis and LI-RADS. *Abdom Radiol* 2018;**43**(1):158–68.
9. Perez-Saborido B, de los Galanes SJ, Meneu-Diaz JC, *et al*. Tumour recurrence after liver transplantation for hepatocellular carcinoma: recurrence pathway and prognostic factors. *Transpl Proc* 2007;**39**(7):2304–7.
10. Jonas S, Bechstein WO, Steinmuller T, *et al*. Vascular invasion and histopathologic grading determine outcome after liver transplantation for hepatocellular carcinoma in cirrhosis. *Hepatology* 2001;**33**(5):1080–6.
11. Gerdes J, Lemke H, Baisch H, *et al*. Cell cycle analysis of a cell proliferation-associated human nuclear antigen defined by the monoclonal antibody Ki-67. *J Immunol* 1984;**133**(4):1710–5.
12. Nakanishi K, Sakamoto M, Yamasaki S, *et al*. Akt phosphorylation is a risk factor for early disease recurrence and poor prognosis in hepatocellular carcinoma. *Cancer* 2005;**103**(2):307–12.
13. Schmilovitz-Weiss H, Tobar A, Halpern M, *et al*. Tissue expression of squamous cellular carcinoma antigen and Ki67 in hepatocellular carcinoma-correlation with prognosis: a historical prospective study. *Diagn Pathol* 2011;**6**:121.
14. Shi W, Hu J, Zhu S, *et al*. Expression of MTA2 and Ki-67 in hepatocellular carcinoma and their correlation with prognosis. *Int J Clin Exper Pathol* 2015;**8**(10):13083–9.
15. Yang C, Su H, Liao X, *et al*. Marker of proliferation Ki-67 expression is associated with transforming growth factor beta 1 and can predict the prognosis of patients with hepatic B virus-related hepatocellular carcinoma. *Cancer Manage Res* 2018;**10**:679–96.
16. Matsui O, Kobayashi S, Sanada J, *et al*. Hepatocellular nodules in liver cirrhosis: hemodynamic evaluation (angiography-assisted CT) with special reference to multi-step hepatocarcinogenesis. *Abdom Imaging* 2011;**36**(3):264–72.
17. Asayama Y, Yoshimitsu K, Nishihara Y, *et al*. Arterial blood supply of hepatocellular carcinoma and histologic grading: radiologic–pathologic correlation. *AJR Am J Roentgenol* 2008;**190**(1):W28–34.
18. Huang Z, Xu X, Meng X, *et al*. Correlations between ADC values and molecular markers of Ki-67 and HIF-1alpha in hepatocellular carcinoma. *Eur J Radiol* 2015;**84**(12):2464–9.
19. Okamura S, Sumie S, Tonan T, *et al*. Diffusion-weighted magnetic resonance imaging predicts malignant potential in small hepatocellular carcinoma. *Dig Liver Dis* 2016;**48**(8):945–52.
20. Nojiri S, Kusakabe A, Fujiwara K, *et al*. Noninvasive evaluation of hepatic fibrosis in hepatitis C virus-infected patients using ethoxybenzyl-magnetic resonance imaging. *J Gastroenterol Hepatol* 2013;**28**(6):1032–9.
21. Kierans AS, Leonardou P, Hayashi P, *et al*. MRI findings of rapidly progressive hepatocellular carcinoma. *Magn Reson Imaging* 2010;**28**(6):790–6.
22. Choi SY, Kim SH, Park CK, *et al*. Imaging features of gadoxetic acid-enhanced and diffusion-weighted MR imaging for identifying cytokeratin 19-positive hepatocellular carcinoma: a retrospective observational study. *Radiology* 2018;**286**(3):897–908.
23. Kawamura Y, Ikeda K, Hirakawa M, *et al*. New classification of dynamic computed tomography images predictive of malignant characteristics of hepatocellular carcinoma. *Hepatol Res* 2010;**40**(10):1006–14.
24. An C, Kim DW, Park YN, *et al*. Single hepatocellular carcinoma: preoperative MR imaging to predict early recurrence after curative resection. *Radiology* 2015;**276**(2):433–43.
25. Asayama Y, Yoshimitsu K, Irie H, *et al*. Poorly versus moderately differentiated hepatocellular carcinoma: vascularity assessment by computed tomographic hepatic angiography in correlation with histologically counted number of unpaired arteries. *J Comput Assist Tomogr* 2007;**31**(2):188–92.
26. Huang X, Xiao Z, Zhang Y, *et al*. Hepatocellular carcinoma: retrospective evaluation of the correlation between gadobenate dimeglumine-enhanced magnetic resonance imaging and pathologic grade. *J Comput Assist Tomogr* 2018;**42**(3):365–72.
27. Fornasa F. Diffusion-weighted magnetic resonance imaging: what makes water run fast or slow? *J Clin Imaging Sci* 2011;**1**:27.
28. Taouli B, Koh DM. Diffusion-weighted MRI of the liver. *Radiology* 2010;**254**(1):47–66.
29. Nakanishi M, Chuma M, Hige S, *et al*. Relationship between diffusion-weighted magnetic resonance imaging and histological tumour grading of hepatocellular carcinoma. *Ann Surg Oncol* 2012;**19**(4):1302–9.
30. Nishie A, Tajima T, Asayama Y, *et al*. Diagnostic performance of apparent diffusion coefficient for predicting histological grade of hepatocellular carcinoma. *Eur J Radiol* 2011;**80**(2):e29–33.
31. Li X, Jiang H, Niu J, *et al*. Correlation of ADC value with pathologic indexes in colorectal tumour homografts in Balb/c mouse. *Chin J Cancer Res* 2014;**26**(4):444–50.
32. Zhang J, Jing H, Han X, *et al*. Diffusion-weighted imaging of prostate cancer on 3T MR: relationship between apparent diffusion coefficient values and Ki-67 expression. *Acad Radiol* 2013;**20**(12):1535–41.
33. Surov A, Meyer HJ, Wienke A. Associations between apparent diffusion coefficient (ADC) and KI 67 in different tumours: a meta-analysis. Part 1: ADCmean. *Oncotarget* 2017;**8**(43):75434–44.
34. Surov A, Caysa H, Wienke A, *et al*. Correlation between different ADC fractions, cell count, Ki-67, total nucleic areas and average nucleic areas in meningothelial meningiomas. *Anticancer Res* 2015;**35**(12):6841–6.
35. Surov A, Meyer HJ, Schob S, *et al*. Parameters of simultaneous ^{18}F-FDG-PET/MRI predict tumour stage and several histopathological features in uterine cervical cancer. *Oncotarget* 2017;**8**(17):28285–96.
36. Zhang Y, Zhang Q, Wang XX, *et al*. Value of pretherapeutic DWI in evaluating prognosis and therapeutic effect in immunocompetent patients with primary central nervous system lymphoma given high-dose methotrexate-based chemotherapy: ADC-based assessment. *Clin Radiol* 2016;**71**(10):1018–29.